# IR-Extended Photoluminescence Mapping of Single-Wall and Double-Wall Carbon Nanotubes

**Konstantin Iakoubovskii,[†] Nobutsugu Minami,\*,[†] Said Kazaoui,[†] Taro Ueno,[†] Yasumitsu Miyata,[†] Kazuhiro Yanagi,[†] Hiromichi Kataura,[†] Satoshi Ohshima,[‡] and Takeshi Saito[‡]**

*Nanotechnology Research Institute, National Institute of Advanced Industrial Science and Technology (AIST), 1-1-1 Higashi, Tsukuba, 305-8565, Japan and Research Center for Advanced Carbon Materials, AIST, 1-1-1 Higashi, Tsukuba, 305-8565, Japan*

A simple and efficient technique is described for measuring photoluminescence (PL) maps of carbon nanotubes (NTs) in the extended IR range (1−2.3 $\mu$m). It consists of preparing an NT/surfactant/gelatin film and measuring PL spectra using a combination of a tunable Ti-sapphire laser excitation and FTIR detection. This procedure has been applied to a wide range of single- and double-wall NTs unveiling chirality and diameter distributions that have so far been very difficult to measure. The problems associated with deducing these distributions are discussed by comparing absorption and PL mapping data for NT samples prepared under different conditions.

## Introduction

The carbon nanotube (NT) is a fascinating "molecule" whose properties strongly depend on its geometric structure. This structure is conventionally classified by chiral indices ($n$, $m$). These indices uniquely determine such important parameters as whether an NT is metallic ($n = m$), semimetallic ($n - m$ is a multiple of 3), or semiconducting (other $n - m$), its energy band structure and diameter.

Nowadays, NTs are produced by a wide variety of growth techniques, such as Co/Mo catalyst-assisted[1] chemical vapor deposition (CoMoCAT CVD), high-pressure CO gas decomposition with Fe catalyst[1] (HiPCO), arc discharge, laser ablation[2] (LA), direct injection pyrolytic synthesis[3,4] (DIPS), and so forth. All these techniques produce NTs with a rather different distribution of (n,m) indices. This distribution strongly depends on the growth conditions (such as catalyst particle size) and thus can show large variations even within the same growth setup. Therefore, there is a clear demand for an easily accessible technique for monitoring the relative concentrations of NTs of certain chirality in a given sample.

Currently, only two techniques are widely employed for this task, high-resolution microscopy and Raman spectroscopy. Unfortunately, both techniques have serious drawbacks: High-resolution microscopy is rather tedious because it monitors a very small number of tubes and is hardly applicable for bundled NTs, which typically dominate most as-grown NT powders. Raman spectroscopy is free from all these complications. However, proper monitoring of the diameter distribution by this technique requires a narrow-line laser, tunable in a wide spectral range, coupled to a high-resolution, IR-extended spectrometer. Only a few such systems exist thus limiting the application of this technique to the proper monitoring of the NT chirality distribution.

In this paper, we discuss three other techniques for deducing the quantitative chirality or diameter distributions of NTs: photoluminescence (PL) excitation[1,3,5,6,7] (PLE), optical absorption, and eventually X-ray diffraction (XRD). The first method has been extensively applied in the past to qualitatively monitor the presence of NTs of certain chiralities in the studied samples. It is somewhat similar to the mentioned Raman excitation mapping, however, PL signals are much stronger and broader, and they are significantly shifted spectrally from the excitation wavelength. As a result, PL mapping systems are much simpler and thus are widely available. Unfortunately, most of them have a limited PL detection range (~0.9−1.6 $\mu$m) and consequently can only detect narrow-diameter (~0.8−1.3 nm) NTs, produced, for example, by HiPCO or CoMoCAT. However, in this work, we describe a simple PL mapping setup with extended IR detection range (1−2.3 $\mu$m). Direct application of this setup to many widely available NT products yielded several interesting and previously unobtainable results, which are also discussed.

## Experiment

**The Extended IR PL Mapping Setup. Advantages of FTIR Detection.** Three spectroscopic techniques are currently utilized for PL mapping of NTs. We shall refer to them as (1) scanning, (2) multichannel detection, and (3) Fourier transform IR (FTIR) methods.

In the first technique, the PL spectrum is dispersed by a grating or prism and is measured by a single-channel detector. Lock-in or single-photon-counting detection allows to achieve superior signal-to-noise (S/N) ratio for this technique. The disadvantage of point-by-point mapping is the long acquisition time (many hours).

This drawback is avoided in the second method, where the whole dispersed PL spectrum is measured by a multichannel detector thus greatly reducing the measurement time. However, lock-in (or other AC) detection cannot be used any longer, thus strongly reducing the S/N ratio for method 2. Currently available multichannel, IR-extended detectors (>1.6 $\mu$m) suffer from large dark currents, even at liquid-nitrogen temperatures, thus yet

---
\* Author to whom correspondence should be addressed. E-mail: n.minami@aist.go.jp.
   [†] Nanotechnology Research Institute.
   [‡] Research Center for Advanced Carbon Materials.

Photoluminescence Mapping of Carbon Nanotubes

*J. Phys. Chem. B, Vol. 110, No. 35, 2006* **17421**

limiting application of method 2 to extended IR PL mapping. Another disadvantage intrinsic to the detection techniques 1 and 2 is a necessity to change gratings and second-order (with respect to the dispersed wavelength) rejection filters during a wide spectral range measurement.

Most of the discussed problems are avoided in the third FTIR detection technique, which has several interesting advantages:

(1) The whole PL spectrum is sent, without the signal-attenuating dispersion, to the detector thus greatly increasing the S/N ratio.

(2) The lack of second-order (vs wavelength) signals facilitates correct, automatic measurements of wide-range spectra (no need to insert order-selecting filters).

(3) Superior spectral resolution ($<1$ cm$^{-1}$) is easily achieved even with the simplest FTIR spectrometers.

(4) The low-frequency noise components, especially problematic for extended IR detectors, do not contribute to the FTIR signal..

(5) The absence of the dispersive element extends the maximal scanning range. However, the absence of the dispersive element also requires much better rejection of the excitation light. Consequently, a tunable laser, rather than a common lamp-monochromator tandem, is best suited for PL excitation in the FTIR−PLE technique.

The FTIR−PLE technique has already been applied to carbon nanotubes.[7] However, the detected PL wavelength was limited to $<1.7$ $\mu$m by the spectral response of the utilized (Ge) detector.

**The FTIR PL Mapping Setup.** Our PL detection system is based on a commercial JASCO FTIR-800 spectrometer, equipped with a broad-band CaF$_2$ beam splitter. Several nitrogen-cooled IR detectors have been tried, including Ge, InGaAs (detection range $<1.7$ $\mu$m), InSb ($<5$ $\mu$m), and extended InGaAs ($<2.3$ $\mu$m, Hamamatsu G7754-01). The best compromise in terms of detection range and S/N ratio was obtained with the last detector, which was thus incorporated into the system. The PL excitation is provided by a Spectra-Physics 3900S CW Ti-sapphire laser, equipped with a broad-band mirror set and pumped by a 5-W Millenia pro 3s laser (532 nm). This laser system remarkably provides ~1 W power, almost constant in the spectral range 700−1020 nm. Besides, the 695−1055 nm range is accessible after additional laser alignment.

**Sample Preparation.** The described above PLE system has been applied to a wide range of NT samples:

(1) Double-wall NTs (DWNTs) produced by CVD technique at AIST or purchased from Carbon Nanotechnologies Incorporated. The DWNT optical properties were rather similar for these two sources and will be presented on the example of AIST samples.

(2) Single-wall NTs (SWNTs) produced by LA[2] or DIPS[3,4] techniques at AIST and arc-discharge powders purchased from Carbolex or Nanoledge companies. The optical spectra will be presented here only for the more representative DIPS, LA, and Carbolex samples.

The NT powders were dispersed for 15 min in 1% D$_2$O solutions of sodium carboxymethylcellulose (CMC) or sodium dodecylbenzene sulfonate (SDBS) using a tip sonifier (20 kHz, ~100 W). CMC was chosen because we found it to be a very efficient dispersant as well as a good film-former for SWNTs,[8] while SDBS is a commonly used dispersant for SWNTs.[3] Several other dispersants have been tried as well, including polymers (poly(vinyl alcohol), hydroxyethylcellulose) and surfactants (sodium dodecyl sulfate, sodium cholate, Triton-X). All these dispersants are suitable for dispersing relatively narrow (CoMoCAT, HiPCO) NTs, but for the wider NTs studied here,
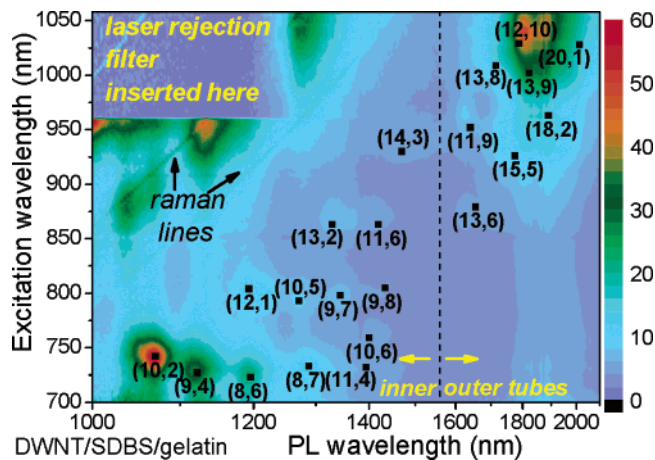


**Figure 1.** PL map for a double-wall NT film prepared from a DWNT/SDBS/gelatin solution. The ($n$, $m$) labeled squares show the chirality assignment using the data of Weisman and Bachilo.[5]

their dispersion efficiency appeared significantly worse, as compared to CMC and SDBS, and therefore the corresponding results will not be presented. The thus prepared dispersions were ultracentrifuged for 5 h at 45 000 rpm (150 000$g$), and the upper 80% supernatant was collected.

Extending the detection range of our PLE setup brought up a "solvent problem": In most NT products, the tubes are present in bundled forms. Bundling strongly broadens and quenches PL signals and thus should be avoided. Numerous unbundling routines are known. Most efficient is dispersing NTs in aqueous solution of a surfactant. Unfortunately, D$_2$O (or water) strongly absorbs light with a wavelength $>1.8$ $\mu$m thus hindering PL detection in that range. On the other hand, drying the sample by casting a thin film brings back the bundling problem. In this work, this obstacle has been overcome by casting thin films from a 1:1 mixture of a 10% gelatin solution and a centrifuged NT/SDBS dispersion on silica substrates. In this procedure,[9] SDBS resulted in efficient micelle-mediated unbundling of NTs, and gelatin, because of gelation, preserved the micelle structure upon water drying. Gelatin brings extra IR absorption for wavelengths $>1.8$ $\mu$m. Therefore, CMC films were used for accurate absorption measurements. These absorption measurements were performed with a commercial Shimadzu UV 3100PC double-beam double-grating spectrometer; 1-cm quartz cells and a D$_2$O reference have been applied for solution samples.

## Results and Discussion

**PL Mapping Results.** All the PL maps presented here were measured from thin-film samples.

**Double-Wall Nanotubes.** The PL map for a DWNT film prepared from DWNT/SDBS/gelatin solution is plotted in Figure 1. The (n,m) labeled squares present the chirality assignment using the widely accepted data of Weisman and Bachilo.[5] In this figure, and in the following figures, the data were slightly (by ~1%) offset to compensate for the matrix-induced peak shift. The unlabeled oval-shaped signals around the top left corner could be assigned to phonon-assisted excitation features.[6] The unusual property of the PL map of Figure 1 is its "bimodal" character, which might be an intrinsic feature of DWNT (compare with Figures 2−4 for SWNTs), that is, there are strong PL peaks at short (bottom left corner) and long (top right corner) excitation/emission wavelengths, but emission is weak in the intermediate range. These peaks could be assigned to the inner and the outer shells of DWNTs, respectively. Note that
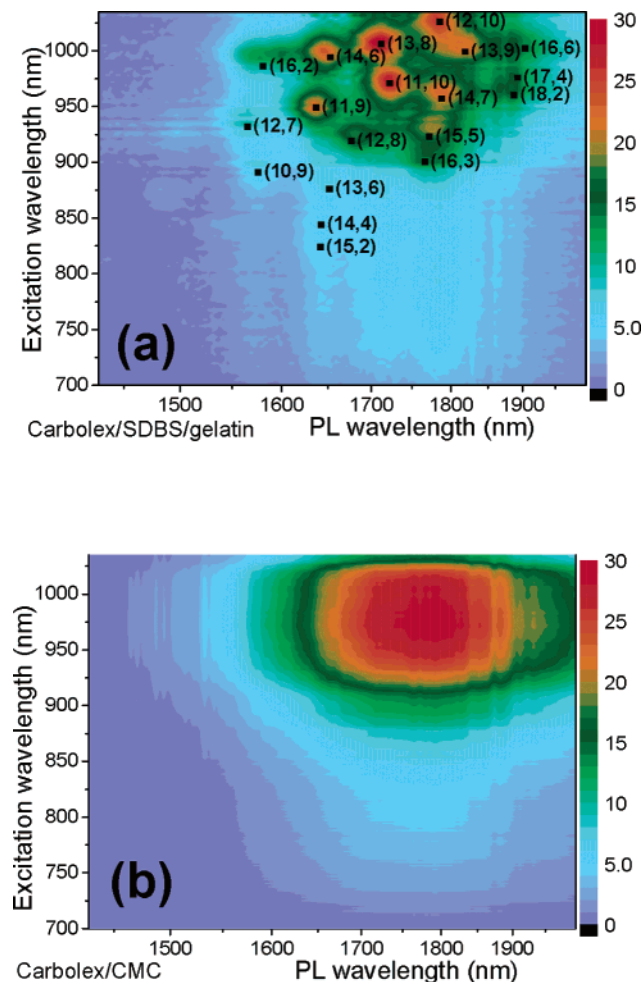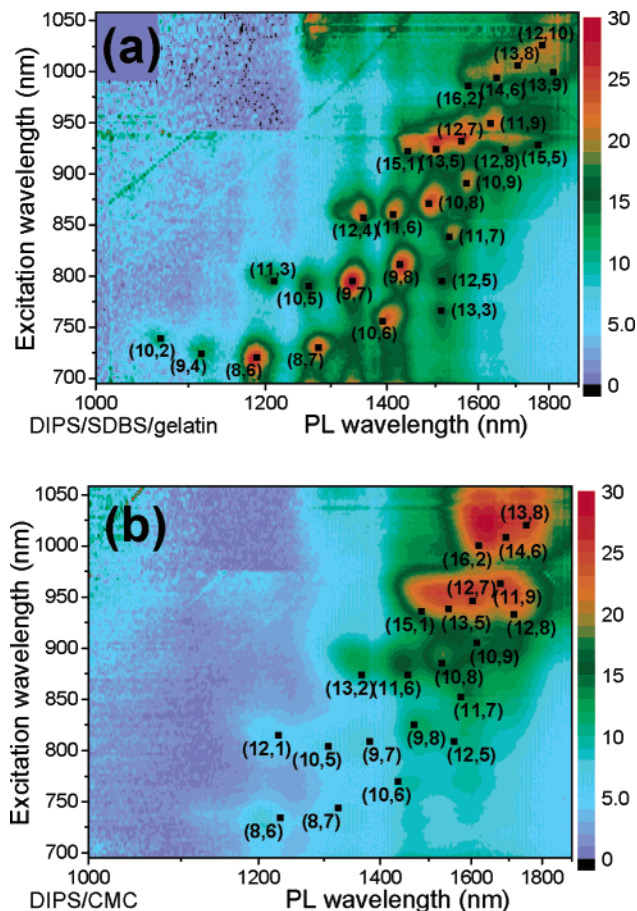
**Figure 2.** PL maps for Carbolex/SDBS/gelatin (a) and Carbolex/CMC (b) films.

extending the PL detection range in this work, combined with the optimized sample preparation routine, resulted in the first mapping of PL from both the inner and the outer shells of DWNTs. Observation of PL from both the inner and the outer tubes suggests that interaction between them is weak in the DWNTs studied here. Only inner-tube PL spectra could be detected previously[10] because of the limited PL detection range. This achievement opens possibilities for further interesting experiments detecting the effect of external perturbations (gas exposure, electrochemical doping, pressure, etc.) on the inner and the outer shells of DWNTs.

The PL assigned in Figure 1 to the inner (or outer) NTs could in principle originate from SWNTs assumingly present in DWNT samples. However, we consider this unlikely because our DWNTs were annealed in air at 500 °C after growth. This annealing should selectively burn SWNTs or at least severely quench PL from SWNTs.

**Single-Wall Nanotubes.** Figures 2a, 2b, 3a, 3b, and 4 present PL maps for Carbolex/SDBS/gelatin, Carbolex/CMC, DIPS/SDBS/gelatin, DIPS/CMC, and LA/SDBS/gelatin films, respectively. Comparison of Figure 2a and b reveals that, for Carbolex SWNTs, the spectral resolution is much worse for CMC than for SDBS dispersant, while the diameter distribution, represented by the PL emission range, remains more or less the same. On the contrary, a similar spectral line width was previously observed for CoMoCAT/CMC and CoMoCAT/SDS, as well as for HiPCO/CMC and HiPCO/SDS systems.[8] To explain this difference, we suggest that CMC isolates single tubes in case



**Figure 3.** PL maps for DIPS/SDBS/gelatin (a) and DIPS/CMC (b) films.
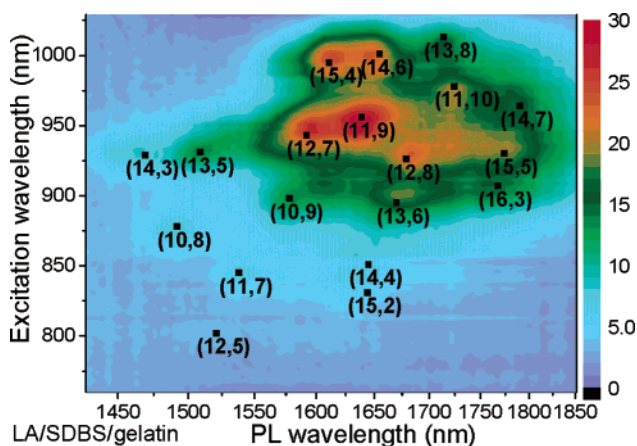


**Figure 4.** PL map for a LA/SDBS/gelatin film.

of CoMoCAT and HiPCO but small bundles in case of Carbolex SWNTs. These small bundles survive the centrifugation and even produce detectable PL. However, this PL is severely broadened (Figure 2b) by the intertube interaction. As to the DIPS SWNTs, PL peaks are also generally broader for CMC than for SDBS (cf. Figure 3a and b). However, the diameter distribution is quite different here; SDBS yields a relatively broad distribution while that for CMC localizes at the longer wavelengths (larger diameters). This difference is discussed below by correlating the PL results with the absorption spectra.

**Comparison of Optical Absorption, PL, and XRD Results for LA SWNTs.** PL mapping of NT/SDBS/gelatin films yielded well-resolved PL/PLE peaks for all the NTs studied, thus allowing their assignment to specific (n,m) indices[5] (Figures

Photoluminescence Mapping of Carbon Nanotubes

*J. Phys. Chem. B, Vol. 110, No. 35, 2006* **17423**
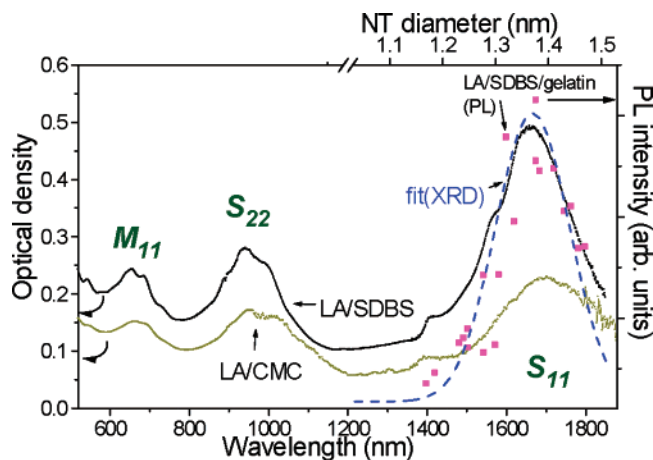


**Figure 5.** Absorption spectra from centrifuged LA/SDBS (top solid curve) and LA/CMC (bottom solid curve) solutions. Note that a much smaller amount of NT was used for CMC solution. Scattered squares present distribution of PL peak intensities (see Figure 4) as a function of PL wavelength (bottom axis) or NT diameter (top axis). Note that the top axis applies only to $S_{11}$ transitions. The dotted line is a Gaussian distribution calculated using the diameter parameters (peak at 1.38 nm, deviation 0.14 nm) deduced from XRD measurements on LA powder.

1−4). This makes it possible to plot distributions of PL peak intensities as a function of PL wavelength or NT diameter. Because of the branching in the Kataura plot,[5] there is no exact and unambiguous relation between the NT diameter and the transition wavelength. Therefore, the NT diameters, used in Figures 5 and 6, are mean values averaged over a large NT ensemble. However, this uncertainty in the diameter/wavelength relation is small for the relatively wide NTs studied here, and it therefore lies within our experimental errors.

The PL peak intensity distribution for the LA/SDBS/gelatin film (Figure 4) is presented by the scatter graph in Figure 5. The top and bottom wide-range curves show absorption spectra from centrifuged LA/SDBS and LA/CMC solutions, respectively. Symbols $S_{11}$, $S_{22}$, and $M_{11}$ assign the absorption peaks to transitions between the first (11) and the second (22) pairs of the van Hove singularities of the density of states in the semiconducting/metallic NTs. An important result in this graph is a close similarity between the $S_{11}$ peak positions measured by absorption or PL from CMC or SDBS solutions or thin films. This agreement suggests that the presented diameter/wavelength distributions are hardly affected by dispersant or measurement technique. Note that similar agreement was observed not only for LA but also for arc-discharge SWNTs (as mentioned above for Carbolex SWNTs).

The above conclusion is further supported by our XRD measurements. Analysis of the XRD data for LA NT powders unambiguously yielded a diameter distribution centered at 1.38 nm with a width of 0.14 nm. Remarkably, a Gaussian distribution (dashed curve), calculated using these parameters (see Figure 5), agrees very well with the optical data. This agreement is rather important because XRD was measured from as-grown powder but with PL and absorption from dispersed SWNTs. It reveals that the dispersion/centrifugation process did not affect the initial NT diameter distribution. Another important detail is that our XRD data were averaged over large NT volumes, which are comparable to those sampled in our optical measurements but are much larger and thus more representative than those scanned by traditional high-resolution microscopy or Raman techniques.

**Comparison of Optical Absorption and PL Results for DIPS SWNTs.** A comparison between optical absorption and
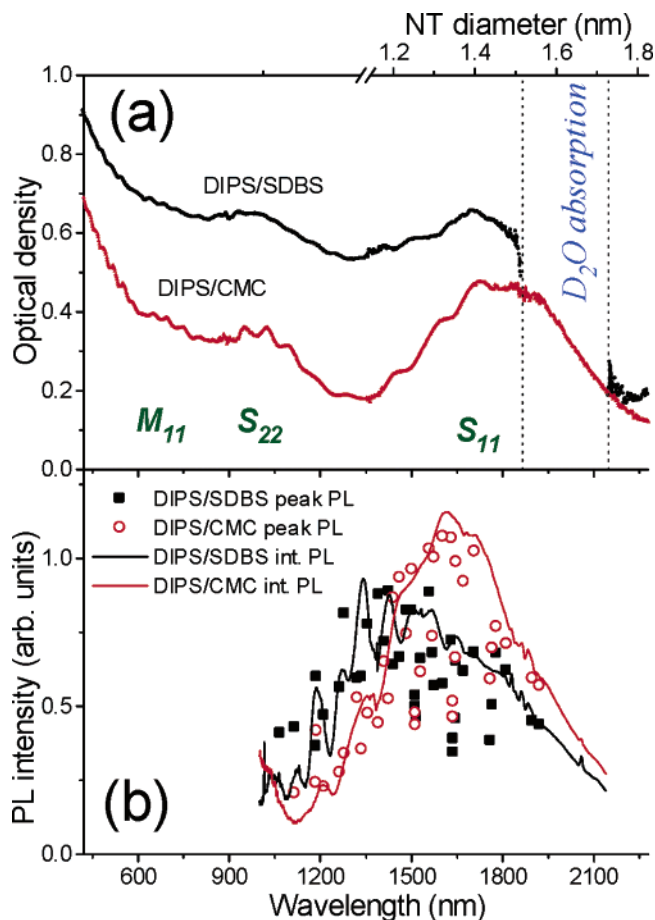


**Figure 6.** (a) Absorption from DIPS/SDBS solution and DIPS/CMC film. (b) Solid squares and open circles present intensity distributions of PL peaks for the DIPS/SDBS/gelatin and DIPS/CMC films, respectively (see Figure 3). Lines are corresponding spectral dependences of PL intensity, integrated over the excitation range.

PL data for DIPS samples is summarized in Figure 6. Here, panel a presents absorption from DIPS/SDBS solution and DIPS/CMC film. Note that some data for DIPS/SDBS are missing at wavelengths strongly absorbed by $D_2O$. Absorption from DIPS/CMC film and solution exhibited the same line shape, therefore, only the former spectrum is shown because it contains no $D_2O$ absorption artifacts. Scatter graphs in Figure 6b present intensity distributions of PL peaks for the DIPS/SDBS/gelatin and DIPS/CMC films (see Figure 3). A significant shift ($\sim$200 nm) is observed between these PL intensity distributions and the corresponding absorption spectra (cf. panels a and b). To check whether this shift could be an artifact of the PL peak analysis, we also plotted (by thin lines) in Figure 6b spectral dependences of PL intensity from the DIPS/SDBS/gelatin and DIPS/CMC films obtained with another, more straightforward procedure, namely, integrating all PL spectra of Figure 3 over the PL excitation range. A close similarity is observed between the PL spectral dependences presented by the scatter graphs and thin lines, thus ensuring the observation of the shift between PL and absorption curves.

As to the origin of this shift, it could be due to the better isolation of narrow tubes, which would increase their PL intensity relative to the (partially bundled) wider tubes thereby shifting the PL distribution. This should explain the difference in PL mapping between DIPS/SDBS and DIPS/CMC dispersions (Figure 3), because such diameter selectivity is more pronounced for SDBS than for CMC. This also corroborates the previous PL mapping work performed for a 1.0−1.6 $\mu$m

range[3]. These isolation aspects should have a rather minor effect on absorption spectra. Therefore, in summary, we suggest that deducing diameter distribution for the studied DIPS nanotubes is much more reliable from absorption than from PL data.

**A Comment on Chirality Dependence of PL Efficiency.** All through this paper, we have implicitly assumed that neither the PL efficiency nor the absorption cross section depends on chirality, which is incorrect, as demonstrated by recent calculation.[11] This chirality dependence probably contributes to the scatter in our PL distribution graphs (see Figure 5 and scatter graphs in Figure 6b). However, this chirality dependence is significant only within one "chirality branch", composed of a few semiconducting nanotubes with the same $2n + m$ values. Averaging over many branches, as it is done in this paper, should partially compensate for the chirality dependence of PL intensity, as confirmed by the close agreement between our PL, absorption, and XRD data for LA SWNTs (Figure 5). It would be highly desirable to correct the PL/absorption intensities for the chirality dependence. Unfortunately, such correction factors are yet only available for narrow-diameter (<1.2 nm) nanotubes.[11]

### Summary and Conclusions

In this paper, we presented a novel experimental technique allowing to map luminescence intensity from carbon nanotubes in the previously unavailable, extended IR range (up to 2.3 $\mu$m). Application of this technique to a range of single- and double-wall carbon nanotubes yielded several important results. In particular, the first PL maps were recorded from DWNTs. Remarkably, PL from both the inner and the outer shells could be detected thus indicating weak interaction between these shells in our DWNT samples. A more detailed study of DWNT is now in progress. In addition, we attempted to assess the suitability of optical absorption and PL techniques for monitoring the diameter/chirality distributions of carbon NTs. The results presented in Figures 5 and 6 suggest that only a combination of these techniques allows us to access those distributions. Optical absorption performed on NT films, prepared using a proper, diameter nonselective, dispersant is probably the easiest monitor of the nanotube diameter distribution; the data of Weisman and Bachilo[5] provide reliable correlation between the $S_{11}/S_{22}$ peak positions and the NT diameter. Unfortunately, peak overlapping in optical absorption hinders exact monitoring of the NT chirality distribution. This distribution can be obtained from PL mapping performed on NT/SDBS/gelatin films. However, such chirality distribution is only reliable in the absence of a significant $S_{11}$ peak shift between absorption and PL data. Our results reveal that such a shift might strongly depend on the NT preparation conditions.

### References and Notes

(1) Bachilo, S. M.; Balzano, L.; Herrera, J. E.; Pompeo, F.; Resasco, D. E.; Weisman, R. B. *J. Am. Chem. Soc.* **2003**, *125*, 11186.

(2) Sakakibara, Y.; Tatsuura, S.; Kataura, H.; Tokumoto, M.; Achiba, Y. *Jpn. J. Appl. Phys.* **2003**, *42*, L494.

(3) Okazaki, T.; Saito, T.; Matsuura, K.; Ohshima, S.; Yumura, M.; Oyama, Y.; Saito, R.; Iijima, S. *Chem. Phys. Lett.* **2006,** *420*, 286.

(4) Saito, T.; Xu, W.-C.; Ohshima, S.; Ago, H.; Yumura, M.; Iijima, S. *J. Phys. Chem. B* **2006**, *110*, 5849.

(5) Weisman, R. B.; Bachilo, S. M. *Nano Lett.* **2003**, *3*, 1235.

(6) Chou, S. G.; Plentz, F.; Jiang, J.; Saito, R.; Nezich, D.; Ribeiro, H. B.; Jorio, A.; Pimenta, M. A.; Samsonidze, G. G.; Santos, A. P.; Zheng, M.; Onoa, G. B.; Semke, E. D.; Dresselhaus, G.; Dresselhaus, M. S. *Phys. Rev. Lett.* **2005**, *94*, 127402.

(7) Lebedkin, S.; Arnold, K.; Henrich, F.; Krupke, R.; Renker, B.; Kappes, M. M. *New. J. Phys.* **2003**, *5*, 140.

(8) Minami, N.; Kim, Y.; Miyashita, K.; Kazaoui, S.; Nalini, B. *Appl. Phys. Lett.* **2006**, *88*, 93123.

(9) Kim, Y.; Minami, N.; Kazaoui, S. *Appl. Phys. Lett.* **2005**, *86*, 73103.

(10) Hertel, T.; Hagen, A.; Talaev, V.; Arnold, K.; Henrich, F.; Kappes, M.; Rosenthal, S.; McBride, J.; Ulbricht, H.; Flahaut, E. *Nano Lett.* **2005**, *5*, 511.

(11) Oyama, Y.; Saito, R.; Sato, K.; Jiang, J.; Samsonidze, G. G.; Gruneis, A.; Miyauchi, Y.; Maruyama, S.; Jorio, A.; Dresselhaus, G.; Dresselhaus, M. S. *Carbon* **2006**, *44*, 873.